



Characterizing vortex beams from a spatial light modulator with collinear phase-shifting holography

JASMINE M. ANDERSEN,¹  SAMUEL N. ALPERIN,¹ ANDREW A. VOITIV,¹  WILLIAM G. HOLTZMANN,¹ 
JULIET T. GOPINATH,^{2,3}  AND MARK E. SIEMENS^{1,*} 

¹Department of Physics & Astronomy, University of Denver, Denver, Colorado 80208, USA

²Department of Electrical, Computer, and Energy Engineering, University of Colorado, Boulder, Colorado 80309, USA

³Department of Physics, University of Colorado, Boulder, Colorado 80309, USA

*Corresponding author: msiemens@du.edu

Received 1 August 2018; revised 28 November 2018; accepted 29 November 2018; posted 30 November 2018 (Doc. ID 341337); published 8 January 2019

We demonstrate collinear phase-shifting holography for measuring complex optical modes of twisted light beams with orbital angular momentum (OAM) generated by passing a laser through a spatial light modulator (SLM). This technique measures the mode along the direction of propagation from the SLM and requires no additional optics, so it can be used to aid alignment of the SLM, to efficiently check for the effects of beam wander, and to fully characterize generated beams before use in other experiments. Optimized error analysis and careful SLM alignment allow us to generate and measure OAM with purity as high as 99.9%. © 2019 Optical Society of America

<https://doi.org/10.1364/AO.58.000404>

1. INTRODUCTION

An optical mode with orbital angular momentum (OAM) is characterized by a helical wavefront with an integer winding number ℓ , leading to an OAM per photon of $\ell\hbar$ [1]. Light's OAM provides a discrete parameter space, with bounds limited only by the numerical aperture of the system [2,3], that has already been utilized in high-torque light-matter interactions [4], quantum entanglement [5,6], and terabit-bandwidth communications based on multiplexing OAM states. [7,8]. These exciting applications require high-purity generation of optical OAM, which is a challenge to measure directly and efficiently in the lab because, while the helical phase of light is an efficient carrier of angular momentum information, it does not directly affect the intensity of the light measured by a camera.

There are many demonstrated methods to characterize and measure light's OAM. The simplest and oldest method is to interfere the beam with a Gaussian reference; the number of azimuthal interference fringes is equal to $|\ell|$ [9]. Diffraction from apertures of various geometries has also been shown to contain information about the nearest-integer ℓ [10,11], even in the presence of other modes [12]. More recent work has shown that the average OAM can be measured quantitatively with a cylindrical lens [13] or by integration of the local OAM density [14]. Finally, modal decomposition methods can take measurements of the OAM power spectrum by log-polar optical transformations [15], diffraction forked grating correlation

filters [16–18], or Fourier analysis of interference patterns [19]. Direct measurement of the optical phase profile is another promising route to full OAM measurement: if the full, complex field of a mode can be measured, then the beam would be completely characterized. Unfortunately, the two traditional methods of measuring a complex mode are insufficient: interferometry using a reference beam with a fixed phase can recover only partial phase information in the form of a forked grating [20] because of sign ambiguity caused by the inverse cosine operation in the recovery of phase information from an interferogram [21], and wavefront sensors are expensive, low resolution, and cannot handle the phase singularities necessarily present within twisted light. Recent work showed that a custom implementation of phase-shifting holography in an interferometer can be used to reconstruct the complex field of a twisted light mode [22]. This work required construction of an interferometer with a separate reference path that can introduce additional phase noise. Other works have utilized similar interferometric methods, including phase-shifting holography, for measurement of complex optical fields such as vortex knots, beams that contain a noninteger vortex structure, and interference of several plane waves from which the phenomenon of laser speckle arises [14,23,24]. In these experiments, a lens imaged the interference between the zero-order and first-diffracted-order beam. While the beams both travel through the same optics, which reduces noise from vibrations, misalignments in the lens can cause distortions in the field, and the

reference beam is not propagated collinearly with the beam under test [25].

In this paper, we show that when a spatial light modulator (SLM) is used to generate complex optical fields with OAM, the beam can be characterized and aligned with collinear phase-shifting holography techniques [21] and no additional optics. We explicitly describe the process of using composite gratings on the SLM, which generates both the studied beam and a copropagating, phase-controlled reference. This complex field measurement is sufficient to decompose the field in a Laguerre Gaussian (LG) basis, providing a fast, direct, and accurate determination of the complete radial mode and OAM mode spectrum. Using this technique, we demonstrate sensitive transverse SLM alignment and complex field measurements, including full ℓ - p spectra from the decomposition, for a variety of OAM modes and a donut mode that does not contain OAM. This inline, collinear technique with no additional optics minimizes phase error and uncertainty from misalignment, and enables straightforward and accurate experimental measurement of small differences in generated optical fields. We also show how to minimize errors from finite size, pixel count, and tilt angle of the detector relative to the beam. The minimization of each of these errors and lack of intermediary optics allow us to confidently generate and measure very high-purity OAM, up to 99.9%.

2. COMMON-PATH PHASE-SHIFTING DIGITAL HOLOGRAPHY OF VORTEX BEAMS

We begin by describing our collinear implementation of phase-shifting digital holography, which is an extension of interferometry that enables phase and amplitude measurements of an arbitrary optical field [21]. This technique requires the measurement of four interferograms with intensities $I(x, y, \phi_R)$ and relative phase ϕ_R between the studied mode and a Gaussian reference beam. The transverse phase of the desired mode, $\Phi(x, y)$, can then be calculated as [21]

$$\Phi(x, y) = \tan^{-1} \left(\frac{I(x, y, \frac{3\pi}{2}) - I(x, y, \frac{\pi}{2})}{I(x, y, 0) - I(x, y, \pi)} \right), \quad (1)$$

illustrated schematically in Fig. 1.

To obtain the optical fields with the needed four phase shifts, we begin by generating a series of four holograms. Each hologram is encoded with the sum of (1) the field of the studied mode superimposed with a plane wave, and (2) a phase reference grating such that the amplitude of the hologram is given by [26]

$$A_H(x, y) = \frac{E_{\text{studied}}(x, y)}{E_{\text{incident}}(x, y)} * e^{\frac{2\pi x}{L}} + e^{\frac{2\pi x}{L} + \phi_R}, \quad (2)$$

where L is the grating constant. We normalize the studied mode by the experimentally measured field incident onto the SLM [27], and subsequently for each value of ϕ_R , these holograms generate the interferograms needed for Eq. (1) in the first diffracted order.

For the case of generating OAM, the plane wave is superimposed with a spiral phase, $e^{i\ell\phi}$, where ℓ is the OAM of the beam [27]. Without the last term in Eq. (2), this creates a hologram such as that shown in the first column of Fig. 1, which does not include a reference beam. The next column of Fig. 1 shows images of the last term in Eq. (2) that generate the reference beams at four phase steps from 0 to $\frac{3\pi}{2}$, as demanded by Eq. (1). Summing columns one and two [i.e., including both terms in Eq. (2)] results in superposition holograms (column three) that each generate the desired mode with a phase-controlled reference beam along a common direction.

Light incident onto one of these holograms results in an interferogram, $I(x, y, \phi_R)$, in the first diffracted order. Each of the four interferograms can be recorded successively on a CCD before combining the images via Eq. (1) to calculate the phase of the desired mode at each pixel location.

To obtain the complete optical field, we must also measure the field amplitude of the beam under test, which is produced by the hologram that contains no additional reference, as in the first column of Fig. 1. This is recorded with a CCD, and by taking the square root of each pixel value, we obtain the amplitude of the mode. This allows for complete measurement of the complex amplitude and phase of the mode being studied.

Illuminating a standard forked diffraction grating, such as the first hologram in Fig. 1, with a Gaussian beam results in a beam with pure OAM, but a superposition of LG radial modes. These beams are referred to as hypergeometric Gaussian (HyGG) modes [26]. Pure LG modes can be produced via an

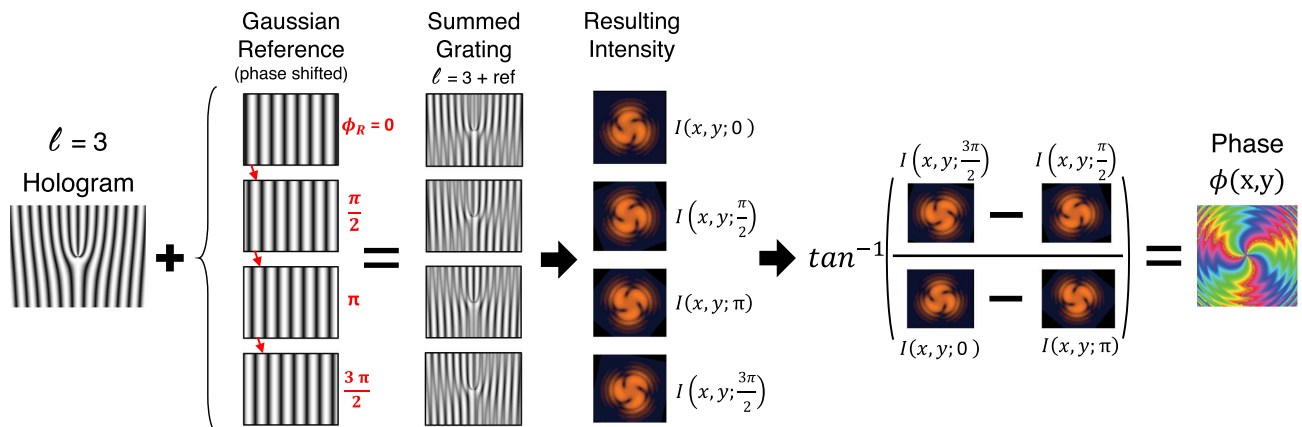


Fig. 1. Schematic representation of phase-shifting digital holography.

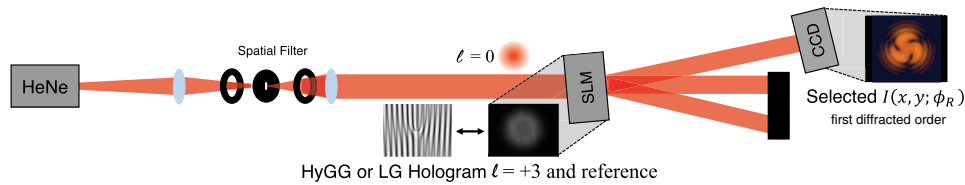


Fig. 2. Experimental schematic. A He–Ne laser passes through a spatial filter onto a SLM from which light in the first diffracted order is collected on a CCD. We project holograms with either HyGG or LG modes plus a phase-controlled reference.

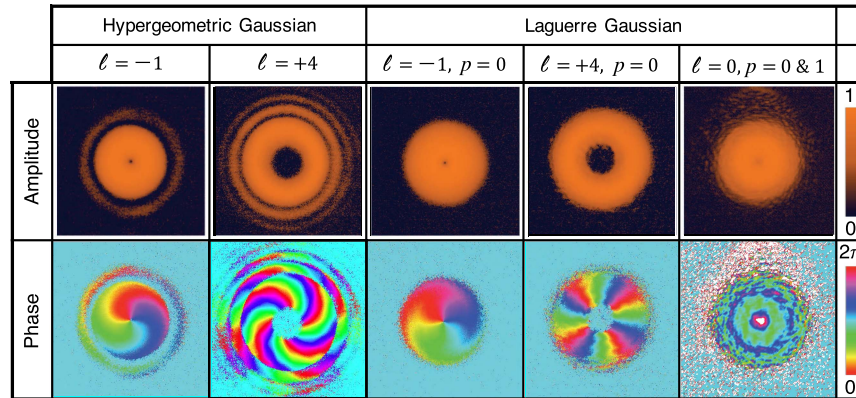


Fig. 3. Experimental measurements of several complex laser modes; phase was measured by collinear phase-shifting digital holography.

additional amplitude mask within the hologram to match the amplitude of the desired LG mode [26]. Each of these LG and HyGG modes have unique phase profiles, even when they carry the same OAM. With this process, we can produce and measure these types of complex optical fields.

For experimental demonstration, a collimated and spatially filtered He–Ne laser is passed through a modified Epson 83H projector LCD panel used as a transmission SLM [28], as shown in Fig. 2. The light in the first diffracted order is measured by a Nikon D5200 camera at an arbitrarily chosen distance of 15% of the Rayleigh range of the generated beam from the SLM. All other diffracted orders are blocked. Figure 3 shows the results of the full complex measurements of HyGG modes with $\ell = +4$ and $\ell = -1$, of LG modes with $\ell = +4$ and $\ell = -1$, and of a “flat donut.”

The measured amplitude and phase are consistent with our expectations. In the amplitude measurements, we see smaller vortex cores in the HyGG beams, in contrast to the single, lowest-order mode in the LG beams with $p = 0$. The phase information also shows a significantly higher amount of curvature in the HyGG modes as compared to the LG modes, as expected due to the additional radial modes present in HyGG beams [26]. The expected topological charge is clearly and directly seen in both the HyGG and LG beams. While a discussion of stability of this measurement is reserved for later, these complete measurements of complex fields give us the ability to quantify the OAM spectrum in each beam.

3. MODAL DECOMPOSITION

Given a direct measurement of the amplitude and phase of an optical field, the field can be computationally decomposed

into any basis. If the LG basis is used, OAM and radial mode power spectra can be determined. This method has distinct advantages over all-optical modal decomposition methods [22], including minimally required data acquisition (one complex beam profile is all that is needed to perform a computational modal decomposition, while an optical decomposition requires separate measurements for each mode), the ability to check other modal bases without acquiring more data, and minimal alignment error. Here, we review the theory for modal decomposition in an LG basis and demonstrate LG modal decomposition of our experimentally measured data shown in the previous section.

A. Theory of Modal Decomposition

We begin by considering an arbitrary complex scalar field Ψ , corresponding to that which can be measured through the techniques described above. This field can be expanded into the sum of LG components, so that

$$\Psi = \sum_{l=-\infty}^{\infty} \sum_{p=0}^{\infty} C_p^{\ell} \text{LG}_p^{\ell}. \quad (3)$$

Orthogonality of LG modes allows for full characterization of the modal composition of Ψ by way of

$$C_p^{\ell} = \int_{\text{All}} \Psi \text{LG}_p^{\ell*} dA. \quad (4)$$

Given experimental measurements of the complex image of arbitrary field Ψ , we can measure C_p^{ℓ} by multiplying that image by a calculated image of $\text{LG}_p^{\ell*}$ and then by summing over all pixels. Thus, after we have a complex image of a field, our method becomes a matter of iterating through digital transmission filters ($\text{LG}_p^{\ell*}$ for all relevant values of ℓ, p) and summing

over all pixels, which allows us to measure C_p^ℓ over a very large portion of the $\{\ell, p\}$ parameter space very quickly, without having to take additional physical measurements for each ℓ .

Based on the decomposition techniques demonstrated in this work and elsewhere [14–19,23,24], one might be tempted to attempt measuring the ℓ power spectrum more directly by using spiral phases alone as a basis for decomposition into an angular momentum distribution. We take a moment to make very clear that for an input field Ψ with arbitrary radial distribution, one cannot measure the angular momentum distribution with spiral phase-only transmission filters. That is to say that in general, the power spectrum coefficient

$$|C_\ell|^2 = \sum_{p=0}^{\infty} \left| \int_{All} \Psi LG_p^{\ell*} dA^2 \right| \neq \left| \int_{All} \Psi e^{-i\ell\phi} dA \right|^2. \quad (5)$$

That this direct spiral decomposition does not work can be understood conceptually as a statement of the nonuniformity of the radial decomposition of a plane wave. One can imagine a beam of the form $\psi = \frac{1}{\sqrt{2}}(LG_{p_1}^{\ell_1} + LG_{p_2}^{\ell_2})$, in which $p_1 \neq p_2$ and $\ell_1 \neq \ell_2$. The angular momentum spectrum of ψ is clearly such that the power is split evenly between the ℓ_1 and ℓ_2 OAM states. However,

$$\begin{aligned} \left| \int_{All} \psi e^{-i\ell\phi} dA \right|^2 &= \left| \frac{1}{\sqrt{2}} \int_{All} (|LG_{p_1}^{\ell_1}| e^{i\ell_1\phi} + |LG_{p_2}^{\ell_2}| e^{i\ell_2\phi}) e^{-i\ell\phi} dA \right|^2 \\ &= \frac{1}{\sqrt{2}} \delta_{\ell\ell_n} \int_{All} |LG_{p_n}^{\ell_n}|^2. \end{aligned} \quad (6)$$

Thus, as the integral of the absolute value of $LG_{p_1}^{\ell_1}$ does not equal that of $LG_{p_2}^{\ell_2}$, the correct angular momentum distribution is not recovered.

B. Example of Modal Decomposition with Experimental Data

Modal decomposition onto an LG basis reveals a full ℓ - p spectrum measurement, and a projection onto the ℓ axis yields the OAM power spectrum. Figure 4 shows results of LG decomposition on three experimentally generated and measured modes: a HyGG with topological charge $\ell = -1$, a LG mode with $\ell = -1$ and $p = 0$, and a composite “flat donut” that is a sum of LG $p = 0$ and $p = 1$ with $\ell = 0$. Power spectra calculations reveal extremely high OAM purity for all of these measurements, on the order of 99.9%. To the authors’ knowledge, this OAM spectral purity is the highest measured to date.

4. ERROR AND STABILITY ANALYSIS

Successfully quantifying the errors affords us high confidence in our ability to accurately measure these OAM modes and confirm our high purities.

A. Finite Window and Pixelation Error Analysis

As was described above in Section 3.A, the modal decomposition of a discretized complex field requires the generation of a set of transformation fields whose centers match that of the field of study. The alignment of the pixel edges of the generated transformation fields in respect to those of the measured image

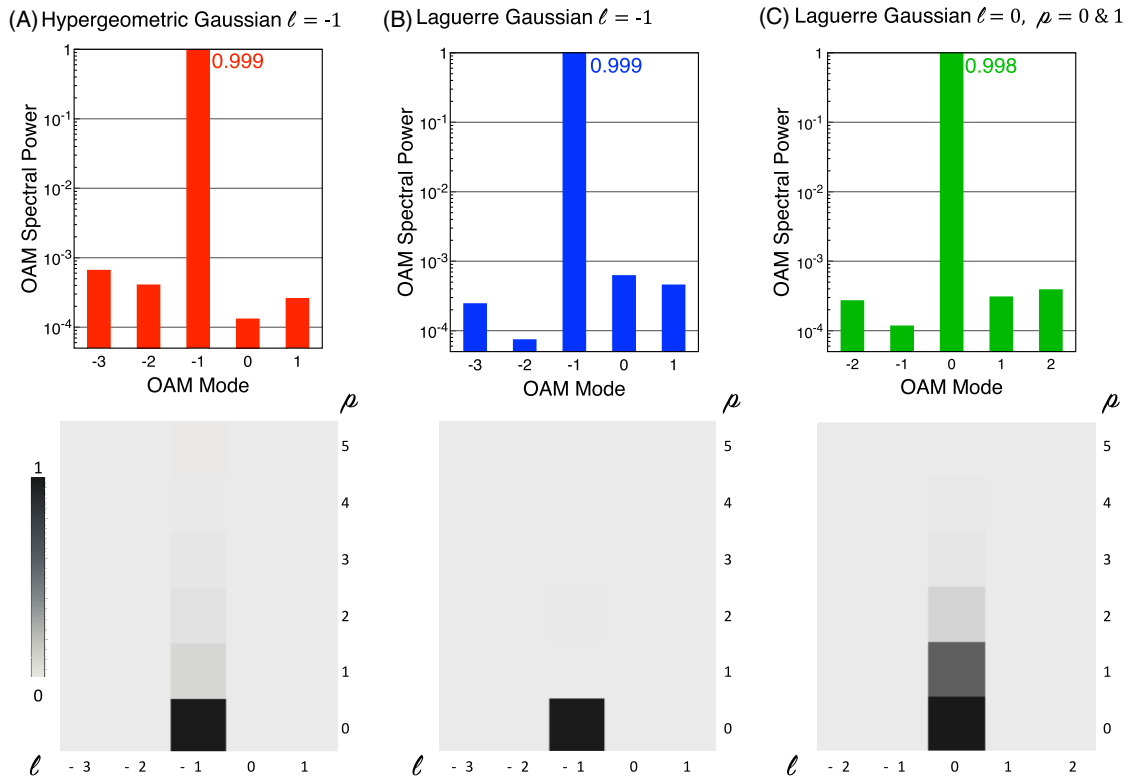


Fig. 4. Results of modal decomposition on three experimentally measured laser modes: (A) a HyGG beam with $\ell = -1$, (B) an LG beam with $\ell = -1, p = 0$, and (C) a composite “flat donut” mode composed of $LG_{\ell=0}^{p=0} - LG_{\ell=0}^{p=1}$. The top graphs show the OAM power spectrum on a logarithmic scale, and the bottom shows the amplitude spectrum in LG_ℓ^p space.

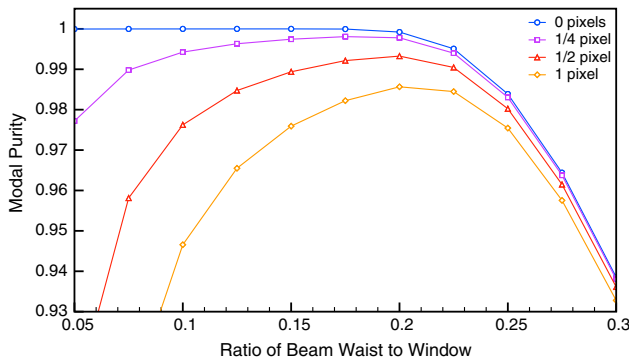


Fig. 5. Modeled modal purity of a pure LG_0^4 mode as a function of beam waist to the total image window. Each curve shows the misalignment error resulting from the measured mode and calculated mode having no relative displacement (blue), a quarter-pixel displacement (purple), a half-pixel displacement (red), and one pixel displacement (orange). We conclude there is an optimal ratio for which the error is mostly negligible, and at which very small (subpixel) misalignment is at its most forgiving. This relative size is approximately $2/5$ of the window, for all values of ℓ . We find slight variations in these errors for different OAM values, but the error-minimizing value of the beam-to-window ratio remains the same.

turns out to be extremely important. However, as the pixel edges are generally fixed for a physical measurement system, and as the alignment of pixel edges can take any place during computational analysis, we show in Fig. 5 that if understood, errors from pixelation are very small even for low-resolution images.

That the errors stemming from pixelation are not a function of resolution as much as they are a function of pixel-edge alignment is surprising, and is a result that can be exploited to achieve high spectral resolution from easy-to-compute, low-resolution data.

Although even inexpensive consumer camera CCDs can be used to record complex images with resolutions on the order of thousands of pixels squared, here we choose to analyze modeled images with only 100 pixels squared to demonstrate that excellent results can be achieved with low-resolution, rapidly computable data. We calculated the spectrum of pure, but discretized, LG modes using different relative displacements between the pixel edge of the modeled image and the transformation filter, and by changing the relative waist size of the mode with respect to the size of the image window. We found that the error in such a measurement is dependent on this relative beam size: too small and the pixel effects are less forgiving, but too large and the beam is clipped by the window. This trend is shown for LG_0^4 in Fig. 5, in which each line represents the measured modal purity as a function of beam size in a fixed window, for different pixel-edge displacements.

B. Detector Tilt Error Measurements

Further measures could be taken into account such as correcting for any potential misalignments in the detector that is measuring the OAM [29]. However, in Fig. 6, we show that our technique is highly insensitive to the tilt of the detector when measuring the OAM. We see only a small deviation in the OAM power spectrum as we increase the tilt of the

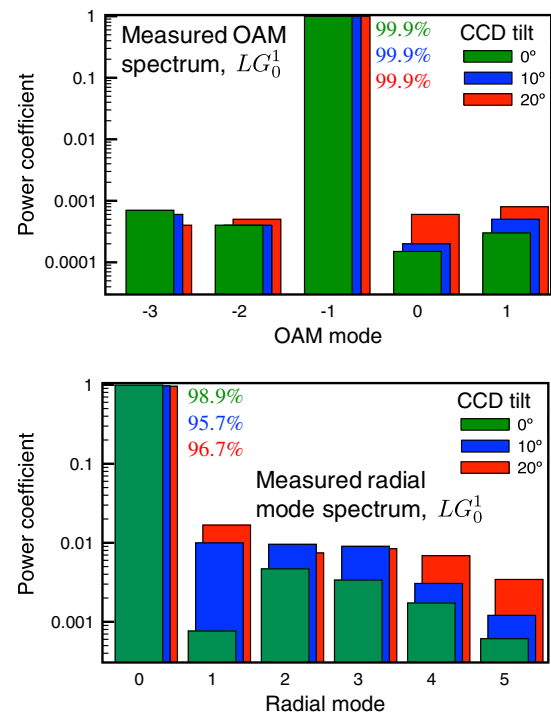


Fig. 6. Measured modal power spectra of a LG_0^1 beam from CCD images taken at 0° , 10° , and 20° of misalignment from the axis of propagation. Top and bottom parts show the same data represented in the OAM (top) and radial (bottom) bases. Data are for integer OAM and radial modes; results for different CCD tilts are slightly offset for clarity.

camera to 10° . When increased to 20° , we see slightly more power in the surrounding modes, but continue to measure a purity of 99.9% in this case. The radial mode spectrum proves to follow the same pattern, but we do observe a decrease in the purity of the $p = 0$ mode. That we observe high OAM purity in the measured mode even in the case of dramatic detector misalignment is indicative of the strength of this technique.

This makes some intuitive sense in that a tilted OAM beam may look oblong in the intensity measured on a camera, but because we also recover the phase, the OAM measurement is preserved at the expense of radial mode purity. These complete error analyses combined with decomposition results demonstrate the robustness of the combined methods of collinear phase-shifting digital holography and our digital modal decomposition.

5. CONCLUSION

In conclusion, we have demonstrated a novel collinear implementation of phase-shifting digital holography to measure the complex field of twisted light. This robust phase recovery allows for fast computational determination of the LG modal spectrum, and therefore the OAM power spectrum. We demonstrate how to mitigate sources of error in such a modal decomposition and find that using these methods, we can reliably measure OAM modal purity up to 99.9%.

Funding. National Science Foundation (NSF) (DMR 1553905, ECCS 1509733, ECCS 1509928, ECCS 1554704).

Acknowledgment. The authors acknowledge useful conversations with Brendan Heffernan, Prof. Lorenzo Marrucci, and Prof. Gabriel Molina-Terriza.

REFERENCES

1. L. Allen, M. W. Beijersbergen, R. J. Spreeuw, and J. P. Woerdman, "Orbital angular momentum of light and the transformation of Laguerre-Gaussian laser modes," *Phys. Rev. A* **45**, 8185–8189 (1992).
2. M. Chen, K. Dholakia, and M. Mazilu, "Is there an optimal basis to maximise optical information transfer?" *Sci. Rep.* **6**, 22821 (2016).
3. S. Restuccia, D. Giovannini, and M. Padgett, "Comparing the information capacity of entangled Laguerre–Gaussian and Hermite–Gaussian modal sets in a finite aperture system," *Opt. Express* **24**, 27127–27136 (2016).
4. N. B. Simpson, K. Dholakia, L. Allen, and M. J. Padgett, "Mechanical equivalence of spin and orbital angular momentum of light: an optical spanner," *Opt. Lett.* **22**, 52–54 (1997).
5. R. Fickler, R. Lapkiewicz, M. Huber, M. P. J. Lavery, M. J. Padgett, and A. Zeilinger, "Interface between path and orbital angular momentum entanglement for high-dimensional photonic quantum information," *Nat. Commun.* **5**, 4502 (2014).
6. A. Mair, A. Vaziri, G. Weihs, and A. Zeilinger, "Entanglement of the orbital angular momentum states of photons," *Nature* **412**, 313–316 (2001).
7. N. Bozinovic, Y. Yue, Y. Ren, M. Tur, P. Kristensen, H. Huang, A. E. Willner, and S. Ramachandran, "Terabit-scale orbital angular momentum mode division multiplexing in fibers," *Science* **340**, 1545–1548 (2013).
8. H. Huang, G. Xie, Y. Yan, N. Ahmed, Y. Ren, Y. Yue, D. Rogawski, M. J. Willner, B. I. Erkmen, K. M. Birnbaum, S. J. Dolinar, M. P. Lavery, M. J. Padgett, M. Tur, and A. E. Willner, "100 Tbit/s free-space data link enabled by three-dimensional multiplexing of orbital angular momentum, polarization, and wavelength," *Opt. Lett.* **39**, 197–200 (2014).
9. J. Vickers, M. Burch, R. Vyas, and S. Singh, "Phase and interference properties of optical vortex beams," *J. Opt. Soc. Am. A* **25**, 823–827 (2008).
10. A. Ambuj, S. Nomoto, H.-H. Shiao, R. Vyas, and S. Singh, "Diffraction of orbital angular momentum carrying optical beams by a circular aperture," *Opt. Lett.* **39**, 5475–5478 (2014).
11. M. E. Anderson, H. Bigman, L. E. E. de Araujo, and J. L. Chaloupka, "Measuring the topological charge of ultrabroadband, optical-vortex beams with a triangular aperture," *J. Opt. Soc. Am. B* **29**, 1968–1976 (2012).
12. A. J. Jesus-Silva, E. J. Fonseca, and J. M. Hickmann, "Study of the birth of a vortex at Fraunhofer zone," *Opt. Lett.* **37**, 4552–4554 (2012).
13. S. N. Alperin, R. D. Niederriter, J. T. Gopinath, and M. E. Siemens, "Quantitative measurement of the orbital angular momentum of light with a single, stationary lens," *Opt. Lett.* **41**, 5019–5022 (2016).
14. J. Leach, E. Yao, and M. J. Padgett, "Observation of the vortex structure of a non-integer vortex beam," *New J. Phys.* **6**, 71 (2004).
15. G. C. G. Berkhout, M. P. J. Lavery, J. Courtial, M. W. Beijersbergen, and M. J. Padgett, "Efficient sorting of orbital angular momentum states of light," *Phys. Rev. Lett.* **105**, 8–11 (2010).
16. G. Molina-Terriza, L. Rebane, J. P. Torres, L. Torner, and S. Carrasco, "Probing canonical geometrical objects by digital spiral imaging," *J. Eur. Opt. Soc.* **2**, 07014 (2007).
17. C. Schulze, A. Dudley, D. Flamm, M. Duparre, and A. Forbes, "Measurement of the orbital angular momentum density of light by modal decomposition," *New J. Phys.* **15**, 073025 (2013).
18. I. A. Litvin, A. Dudley, F. S. Roux, and A. Forbes, "Azimuthal decomposition with digital holograms," *Opt. Express* **20**, 10996–11004 (2012).
19. S. Ramachandran and P. Kristensen, "Optical vortices in fiber," *Nanophotonics* **2**, 455–474 (2013).
20. Y. Fang, Q. Lu, X. Wang, W. Zhang, and L. Chen, "Fractional-topological-charge-induced vortex birth and splitting of light fields on the submicron scale," *Phys. Rev. A* **95**, 023821 (2017).
21. I. Yamaguchi, "Phase-shifting digital holography," *Opt. Lett.* **22**, 1268–1270 (1997).
22. A. D. D'Errico, R. D. Amelio, B. Piccirillo, F. Cardano, L. Marrucci, D. Fisica, N. Federico, C. Universitario, S. Angelo, and V. Cintia, "Measuring the complex orbital angular momentum spectrum and spatial mode decomposition of structured light beams," arXiv: 1706.4788v1 (2017).
23. J. Leach, M. R. Dennis, J. Courtial, and M. J. Padgett, "Vortex knots in light," *New J. Phys.* **7**, 55 (2005).
24. K. O'Holleran, M. J. Padgett, and M. R. Dennis, "Topology of optical vortex lines formed by the interference of three, four, and five plane waves," *Opt. Express* **14**, 3039–3044 (2006).
25. J. Visser and G. Nienhuis, "Orbital angular momentum of general astigmatic modes," *Phys. Rev. A* **70**, 013809 (2004).
26. V. V. Kotlyar, R. V. Skidanov, S. N. Khonina, and V. A. Soifer, "Hypergeometric modes," *Opt. Lett.* **32**, 742–744 (2007).
27. T. W. Clark, R. F. Offer, S. Franke-Arnold, A. S. Arnold, and N. Radwell, "Comparison of beam generation techniques using a phase only spatial light modulator," *Opt. Express* **24**, 6249–6264 (2016).
28. D. Huang, H. Timmers, A. Roberts, N. Shivaram, and A. S. Sandhu, "A low-cost spatial light modulator for use in undergraduate and graduate optics labs," *Am. J. Phys.* **80**, 211–215 (2012).
29. P. Zhao, S. Li, Y. Wang, X. Feng, C. Kaiyu, L. Fang, W. Zhang, and Y. Huang, "Identifying the tilt angle and correcting the orbital angular momentum spectrum dispersion of misaligned light beam," *Sci. Rep.* **7**, 7873 (2017).